PAPER

In situ study on surface roughening in radiation-resistant Ag nanowires

IOP Publishing Nanotechnology

Nanotechnology **29** (2018) 289501 (1pp) https://doi.org/10.1088/1361-6528/aac0e2

Corrigendum: *In situ* study on surface roughening in radiation-resistant Ag nanowires (2018 *Nanotechnology* **29** 215708)

Z Shang[1], Jin Li[1], C Fan[1], Y Chen[2], Q Li[1], H Wang[1,3], T D Shen[4] and X Zhang[1]

[1] School of Materials Engineering, Purdue University, West Lafayette, IN 47907, United States of America
[2] MPA-CINT, Los Alamos National Laboratory, Los Alamos, NM 87545, United States of America
[3] School of Electrical and Computer Engineering, Purdue University, West Lafayette, IN 47907, United States of America
[4] State Key Laboratory of Metastable Materials Technology and Science, Yanshan University, Qinhuangdao 066004, People's Republic of China

E-mail: xzhang98@purdue.edu

Received 20 April 2018
Accepted for publication 27 April 2018
Published 15 May 2018

1. On page 3, in the caption of figure 1, on the first line, '(a)–(d)' should be modified to '(a)–(c)'. And '(a′)–(d′)' should be changed to '(a′)–(c′)'.
2. On page 8, at the end of the Discussion section, the sentence 'This study suggests that metallic nanowires may have significantly improved radiation tolerance compared to bulk counterparts in general. Free surfaces combined with size effects are compelling approaches to design advanced radiation tolerant materials [62].' should be added.
3. On page 8, at the beginning of the Acknowledgments section, after the first sentence, 'ZS is partially supported by NSF-DMR 1611380.' should be added. After the second sentence, 'HW acknowledges financial support from the ONR N00014-16-1-2778.' should be added.
4. On page 10, at the end of the References, '[62] Zhang X, Hattar K, Chen Y, Shao L, Li J, Sun C, Yu K, Li N, Taheri M L, Wang H, Wang J, Nastasi M 2018 Radiation damage in nanostructured materials *Prog. Mater. Sci.* **96** 217–312' should be added.

ORCID iDs

Z Shang https://orcid.org/0000-0002-2974-2599

IOP Publishing Nanotechnology
Nanotechnology 29 (2018) 215708 (10pp) https://doi.org/10.1088/1361-6528/aab537

In situ study on surface roughening in radiation-resistant Ag nanowires

Z Shang[1], Jin Li[1], C Fan[1], Y Chen[2], Q Li[1], H Wang[1,3], T D Shen[4] and X Zhang[1]

[1] School of Materials Engineering, Purdue University, West Lafayette, IN 47907, United States of America
[2] MPA-CINT, Los Alamos National Laboratory, Los Alamos, NM 87545, United States of America
[3] School of Electrical and Computer Engineering, Purdue University, West Lafayette, IN 47907, United States of America
[4] State Key Laboratory of Metastable Materials Technology and Science, Yanshan University, Qinhuangdao 066004, People's Republic of China

E-mail: xzhang98@purdue.edu

Received 12 December 2017, revised 21 February 2018
Accepted for publication 8 March 2018
Published 28 March 2018

Abstract

Metallic materials subjected to heavy ion irradiation experience significant radiation damage. Free surface is a type of effective defect sinks to improve the radiation resistance in metallic materials. However, the radiation resistance of metallic nanowires (NWs) is largely unknown. Here we show, via *in situ* Kr ion irradiations in a transmission electron microscope, Ag NWs exhibited much better radiation resistance than coarse-grained Ag. Irradiation-induced prominent surface roughening in Ag NWs provides direct evidence for interaction between defect clusters and free surface. Diameter dependent variation of the surface roughness in irradiated Ag NWs has also been observed. This study provides insight on mechanisms of enhanced radiation resistance via free surfaces in metallic NWs.

Supplementary material for this article is available online

Keywords: Ag nanowire, *in situ* irradiation, radiation damage, surface roughness

(Some figures may appear in colour only in the online journal)

1. Introduction

As one of the clean, reliable and sustainable energy sources, nuclear energy provides more than 13% of the electrical power worldwide in the past decades [1, 2]. Next generation nuclear reactor concepts require advanced materials with superior radiation resistance [3, 4]. Heavy ion irradiations often induce the formation of various types of damages such as Frenkel pairs, dislocation loops, stacking fault tetrahedrons, cavities and precipitates seriously degrading the properties of materials [5–7]. One of the feasible approaches to mitigate radiation damage in materials is to increase their self-healing capacity by introducing a large number of neutral defect sinks, including high angle grain boundaries, twin boundaries (TB), interfaces and free surfaces [8–16].

Free surfaces are perfect defect sinks because of their unsaturated capacity to capture irradiation-produced defects. Therefore, materials with high surface-to-volume ratios, such as nanowires (NWs) and nanoporous (NP) materials, are anticipated to have a better radiation resistance compared with their coarse-grained (CG) counterparts [14, 15, 17]. Radiation responses of NP Ag, Au and Mg have been investigated [14, 16–19]. In general, NP metals have shown enhanced radiation resistance than CG counterparts. For instance, the defect density and size in irradiated NP metals are smaller than those in CG metals [14, 16, 18, 19]. In addition, the diffusivity of defect clusters is less than that in CG metals [14, 16]. A recent study shows that nanopores in NP Au shrink during *in situ* Kr ion irradiation due to the frequent absorption of irradiation induced defects by free surfaces [16, 19]. Furthermore, the pore shrinkage rate decreases during radiation at elevated temperatures. Mechanical behaviors of metallic NWs have also been investigated [20, 21]. Zhu *et al* performed an *in situ* tensile testing on Ag NWs with diameters ranging from 34 to

130 nm and found that tensile strength increased as NW diameter decreased [20]. Moreover, Filleter *et al* discovered an obvious size-dependent strain hardening phenomenon in penta-twinned Ag NW, stating that smaller NWs exhibit higher strain hardening capacity [21].

Although mechanical behaviors of NWs have been intensively studied, radiation studies on NWs remain scarce. Previous *in situ* irradiation study on ZnO NWs showed that NWs with sufficiently small diameters are nearly immune to radiation damage owing to the existence of defect denuded zones near free surfaces [15]. A recent molecular dynamics (MD) simulation study on Au NWs showed that the primary knock-on atoms (PKAs) with a kinetic energy of 10 keV can lead to the formation of craters on the surface of NWs due to microexplosion of hot atoms produced by displacement cascades and finally causes surface morphology variation [22]. Ag NWs are appealing candidate for transparent electrode fabrication as a result of their flexibility, mechanical properties, and higher electrical and thermal conductivities [23]. Irradiation-induced defects and surface morphology variation may influence the electrical and mechanical properties of NWs. Nano-welding techniques such as electron/ion beam irradiation are used to improve the electrical conductivity by increasing the contacting area at wire-to-wire junctions [24, 25]. During the welding process, controlling defect density and dimensional stability of NWs is essential to obtain high electrical conductivity similar to their bulk counterpart for application in microelectronic devices. In addition, mechanical properties of NWs are also sensitive to dimensional variations. Prior studies have shown that the surface morphology of NWs, such as surface grooves, can affect their mechanical behaviors [26, 27].

In this paper, *in situ* Kr ion irradiation studies were performed on CG Ag and NW Ag in a transmission electron microscope (TEM) at room temperature. Ag NWs exhibit better radiation tolerance compared to CG Ag. Size-dependent surface roughening induced by irradiation was observed experimentally in Ag NWs for the first time. The surface roughening is attributed to frequent interactions between radiation induced defect clusters and free surfaces. This study sheds light on the possible application of defect-free and high electrical conductivity NWs for potential electronic devices in future advanced nuclear reactors.

2. Methods

Ag NWs with diameters ranging from 35 to 75 nm in water solution synthesized by polyol process were procured from Nanostructured & Amorphous Materials, Inc. TEM samples for *in situ* irradiation in this study were prepared by lifting the as-received Ag NWs onto Cu grids coated with carbon films and then were dried in air. All the Ag NWs are randomly distributed on the carbon films. TEM sample disks of CG Ag were cut from Ag sputter target, and then were prepared by polishing, dimpling and argon ion milling at a low energy (3.5 keV). *In situ* irradiation experiment on CG Ag and NW Ag was performed in the Intermediate Voltage Electron Microscopy (IVEM) facility at Argonne National Laboratory. The facility consists of a HITACHI H-9000NAR microscope operated at 200 keV and an ion accelerator with an ion-beam incidence on the specimen at 30° with respect to the electron beam, and the ion beam spot size was estimated to be ~1.5–2 mm [28]. The radiation damage level in unit of displacements per atom (dpa) was calculated by using Stopping and Range of Ions in Matter computer program with Kinchin–Pease method, and the displacement energy of 40 eV was used for Ag in this calculation [29–31]. The TEM samples were irradiated to 2×10^{13} (~0.1 dpa), 4×10^{13} (~0.2 dpa), 1×10^{14} ions cm^{-2} (~0.5 dpa) and finally a maximum fluence of 2×10^{14} ions cm^{-2} (~1 dpa) at room temperature with 1 MeV Kr^{++} ion beam, and a CCD camera was used to record the video of microstructural evolution at a rate of 15 frames s^{-1}. The diameter of the irradiated NW was measured at different places (at least 10 positions) along the NW. Then an average value $\overline{D}$ was calculated as the NW diameter.

3. Results

The microstructural evolutions of CG Ag and NW Ag during irradiation up to 1 dpa captured by TEM are shown in figure 1. Before irradiation only a few preexisting defect clusters were observed in CG Ag (figure 1(a)), while the Ag NWs were almost defect-free (figure 1(a′)). The diameters of the as-received Ag NWs are less than 100 nm, and most of the NWs are transparent to electron beam. The inserted selected area diffraction patterns show the single crystalline and polycrystalline characteristics in CG Ag and Ag NWs, respectively. After irradiation for 0.5 dpa. CG Ag was swarmed with large numbers of irradiation induced defect clusters labeled by white arrows (figure 1(b)). Compared to CG Ag only a few defect clusters were discovered in Ag NWs, meanwhile the free surface morphology of NWs became rough with the increasing radiation dose (figure 1(b′)), indicating the onset of an obvious surface roughening phenomenon during 0–0.5 dpa. A further increase in radiation dose up to 1 dpa did not significantly change the average defect cluster density in CG Ag and Ag NWs, but made the free surface in Ag NWs rougher, as shown in figures 1(c) and (c′).

To study the surface roughening phenomenon in Ag NWs, NWs with diameters (D) of 37, 45 and 81 nm were selected for further investigation. TEM micrographs of these NWs before and after irradiation for 1 dpa are shown in figure 2. After irradiation, humps and valleys indicating surface roughening were frequently observed. Inner diameter (D_i) and exterior diameter (D_e) are defined as the radial distance between two deepest valleys and two highest humps, respectively. Surface roughness (R) is obtained by measuring the average radial height difference between an adjacent hump and valley. For the unirradiated NWs, it is reasonable to assume that $D_i = D_e = D$, because of their relatively smooth free surfaces. For the 37 nm NW in figure 2(a1), D_i remained the same but D_e increased to 40 nm, leading to an R value of 2 nm after irradiation to 1 dpa, as shown in figure 2(a2). For

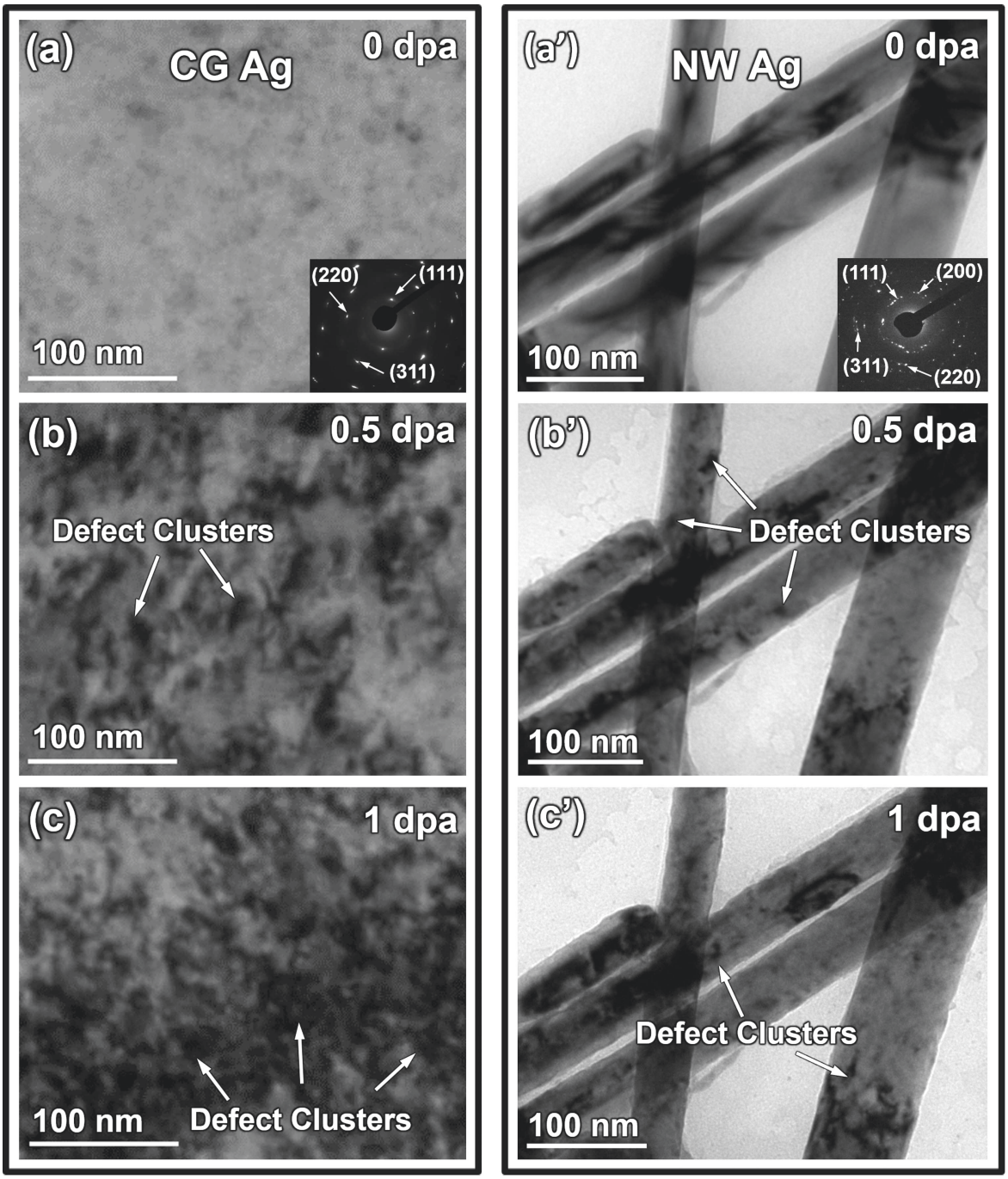

Figure 1. Comparisons of microstructural evolutions in CG (a)–(d) and NW (a′)–(d′) Ag during the *in situ* Kr ion irradiation at room temperature up to 1 dpa. (a)–(a′) Both annealed CG Ag and NW Ag were almost defect free. The inserted selected area diffraction (SAD) pattern shows the polycrystalline characteristics of NW Ag. (b)–(b′) By 0.5 dpa, there was a much more pronounced increase in the number of defect clusters in CG Ag than that in NW Ag. Only a few defect clusters were observed in NW Ag. (c)–(c′) By 1 dpa, the defect density in CG Ag appeared much larger than that in NW Ag. An obvious surface morphology variation in NW Ag was also observed.

the NW with diameter of 45 nm in figure 2(b1), D_i remained nearly unchanged, but D_e increased prominently to 50 nm and R has had a maximum value of 3.5 nm after irradiation. For the irradiated 81 nm NW in figure 2(c1), D_i was ∼80 nm, whereas D_e increased to 88 nm, and R reached a maximum of ∼4 nm.

Irradiation induced evolutions of wire diameter, defect cluster density, defect size, and surface roughness are systematically investigated. As shown in figure 3(a), the average diameters of most NWs increased slightly, by ∼5%, with radiation dose to 1 dpa. The error bars of the measured average diameters tend to increase with radiation dose gradually as well, indicating the wire surface morphology variations during irradiation. The defect cluster density in CG Ag increased dramatically during initial radiation to 0.1 dpa, and then reached saturation, $\sim 2 \times 10^{23}\ m^{-3}$ (figure 3(b)). However, defect cluster densities of Ag NWs with diameters of 37 nm, 45 nm and 81 nm started to saturate at ∼0.2 dpa, at

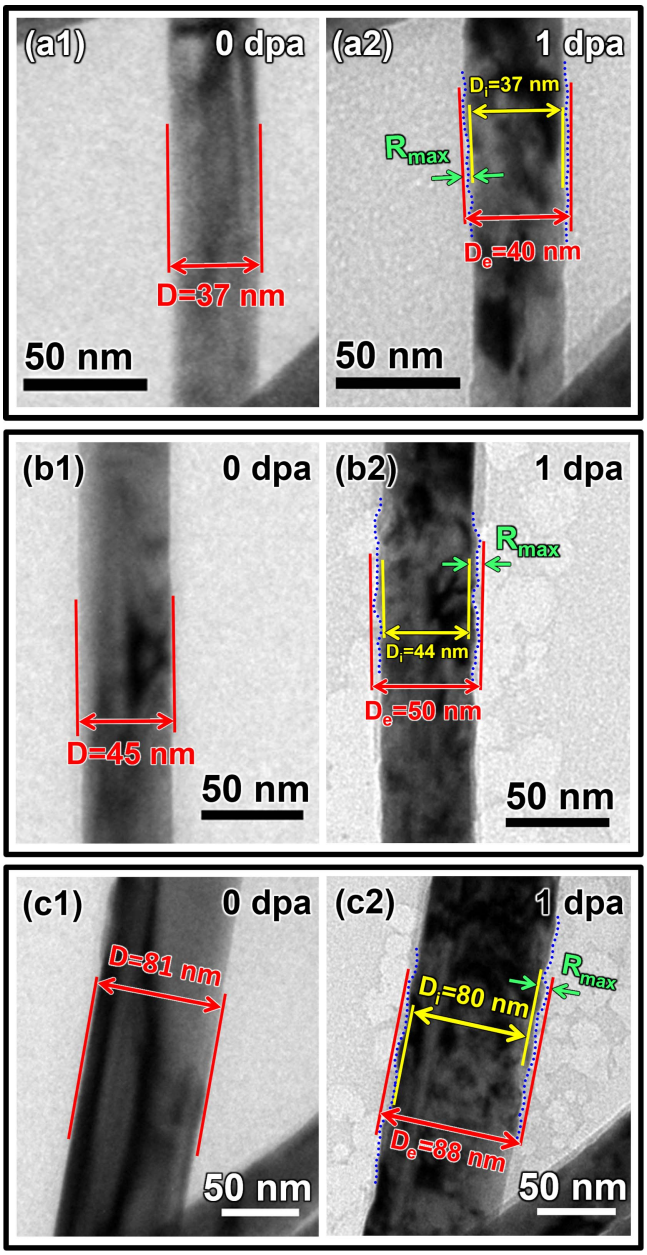

Figure 2. Surface morphology variation in Ag NWs of (a1), (a2) 37 nm, (b1), (b2) 45 nm and (c1), (c2) 81 nm in diameter before and after Kr ion irradiation to 1 dpa. Humps and valleys formed on the surface of NWs after irradiation. Inner diameter (D_i) was determined by the radial distance between two deepest valleys and external diameter (D_e) was measured by the radial distance between two highest humps. Surface roughness (R) is the average radial height difference between adjacent hump and valley.

a defect cluster density of 7, 8 and 12 $\times$ 10^{22} m^{-3}, respectively. The saturated defect cluster density of NW Ag is at least 40% lower than that in irradiated CG Ag. Figure 3(c) illustrates that both surface roughness and saturated defect cluster density increase monotonically with wire diameters. Statistic studies in figures 3(d)–(f) show that the average defect cluster size is 12 nm in 81 nm Ag wires, 11 nm in 45 nm Ag NWs, and 7 nm in 37 nm Ag NWs.

In situ radiation videos reveal frequent interactions of irradiation induced defect clusters with free surface in Ag NWs, causing the roughening of wire surfaces. Some typical examples for the formation of dimples on the surface are shown in figures 4(a1)–(a3) (see supplementary video 1 is available online at stacks.iop.org/NANO/29/215708/mmedia for more details). Two irradiation induced defect clusters D1 and D2 formed near the free surface in the 45 nm diameter Ag NW as shown in figure 4(a1). By 34 s, the two clusters combined into a larger defect cluster D3 (~10 nm in diameter) (figure 4(a2)). After lingering near the free surface for 40 s, D3 was absorbed by the surface, forming a small dimple and leaving behind three smaller defect clusters, as indicated in figure 4(a3). On the other hand, figures 4(c1)–(c3) recorded the formation of a hump (between two pre-existing humps) due to the interaction of defect clusters with free surface (see supplementary video 2 for more details). In a Ag NW with 83 nm diameter, an irradiation induced defect cluster D4 (~15 nm in diameter) formed near two preexisting humps H1 and H2 on the free surface in figure 4(c1). By 40 s, D4 dissociated into two smaller defect clusters D5 and D6 (~8 nm in diameter), as shown in figure 4(c2). Soon after the dissociation, it appeared that both D5 and D6 interacted with the free surface, leading to the formation of a new hump H3 between the preexisting H1 and H2. Meanwhile a larger defect cluster D7 (~13 nm in diameter) was left behind. The schematic diagrams illustrating the interaction of irradiation induced defects with NW surface within the area labeled by the white rectangular square are shown in figures 4(b1)–(b3) and (d1)–(d3).

4. Discussion

4.1. Defect cluster densities in NWs with different diameters

Compared with CG Ag, Ag NWs have a better radiation resistance because free surfaces act as defect sinks in eliminating irradiation induced point defects and defect clusters [14–16, 32]. For a Ag NW with diameter of D and length of L, the surface-to-volume ratio can be calculated by: $(\pi DL)/(\pi LD^2/4) = 4/D$. Therefore, decreasing the diameter of NWs can increase the fraction of atoms on free surface. During irradiation, defects formed near free surface in NW Ag will experience an image force normal to the surface, the magnitude of which is proportional to $1/h$, where h is the nearest distance between the defect cluster and the surface [33]. Hence defects that are close to the free surface can be attracted to the surface by the image force and subsequently be absorbed by the free surface, forming surface affected zones (SAZs), wherein defect density may be lower than crystal interior [14].

Compared with grain boundaries and TB, free surfaces are commonly considered as ideal defect sinks with unsaturable sink capacity [17]. He bubble denuded zones ranging from 0 to 24 nm have been discovered near grain boundaries with various inclination angles in Cu irradiated with He ions at high temperature [10]. Besides, twin boundary affected zones with widths ranging from 5 to 15 nm were also observed in nanotwinned Ag irradiated by Kr ions at both room and elevated temperatures [34, 35]. A recent *in situ* irradiation study showed that the width

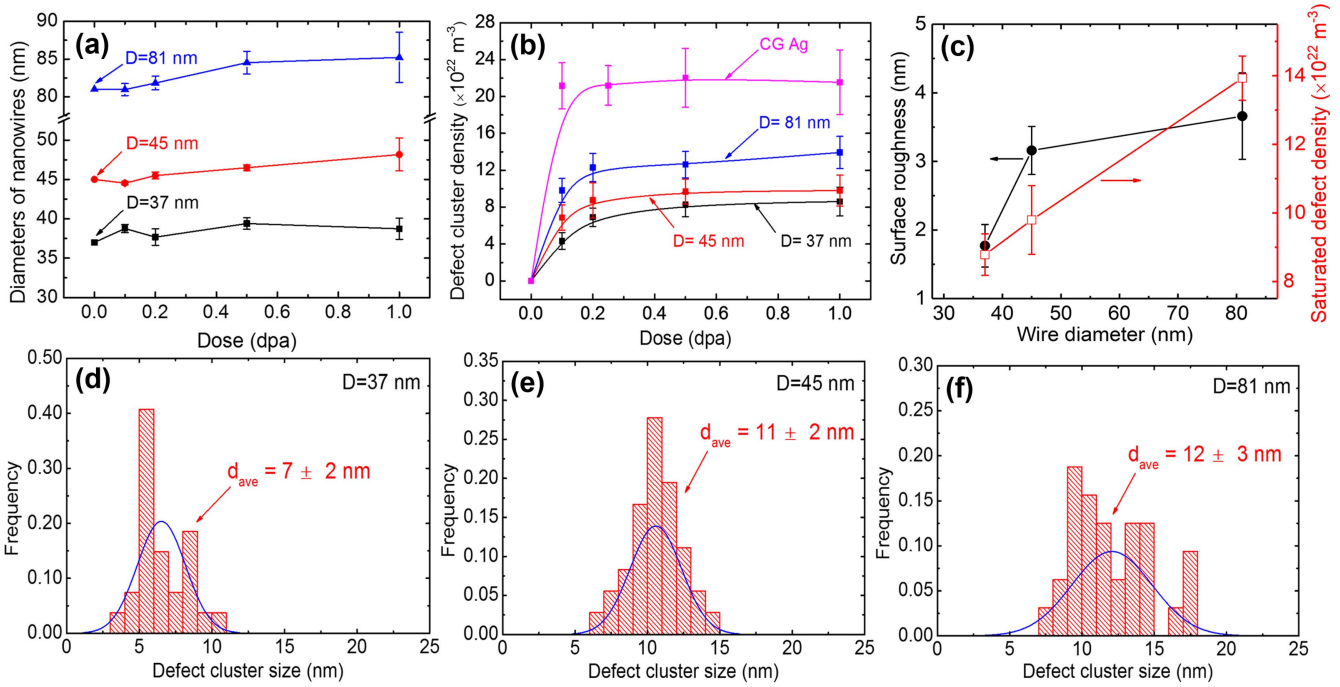

Figure 3. (a) Diameter (D) variation with radiation dose up to 1 dpa in several Ag NWs. The average diameter of each NW increased slightly. The error bar increased prominently with radiation dose, indicating changes in surface roughness. (b) Variation of average defect density in CG Ag and NW Ag of 37 nm, 45 nm and 81 nm in diameter with radiation dose. The average defect density in CG Ag is two times larger than that in NW Ag. In addition, the defect density in both CG Ag and NW Ag reached a saturation after irradiation to 0.2 dpa. (c) Both surface roughness and saturated defect density increased monotonically with wire diameter. Comparison of statistical distribution of defect size in NW Ag with diameters of (d) 37 nm, (e) 45 nm and (f) 81 nm indicates that the average defect cluster size increases with wire diameter.

of SAZ is ~25 nm in ZnO NWs and is independent of the NW diameter so that the NW with a diameter smaller than 50 nm is almost defect-free [15]. For irradiated Ag NW with a smaller diameter such as 37 nm, it is possible that the entire NW is affected by SAZs. The SAZs may be responsible for the differences in the saturated defect cluster density in NWs with different diameters.

In the present study, the statistics data indicate that both the density and size of defect clusters in thicker NWs are greater than those in thinner wires. According to the kinetic rate theory, the variation of vacancy and interstitial concentrations with time can be expressed by the following equations [5, 36]:

$$\partial C_v/\partial t = K_0 - K_{\mathrm{rec}} C_i C_v - k_{sv}^2 D_v C_v \quad (1)$$

$$\partial C_i/\partial t = K_0 - K_{\mathrm{rec}} C_i C_v - k_{si}^2 D_i C_i, \quad (2)$$

where C_v and C_i are the vacancies and interstitials concentrations, respectively. K_0 is the point defect production rate. K_{rec} is the vacancy-interstitial recombination coefficient and t is the irradiation time. D_v and D_i are the diffusivity coefficients for vacancies and interstitials. k_{sv}^2 and k_{si}^2 are the free surface sink strengths for vacancies and interstitials, respectively. Since free surface is considered as neutral defect sinks, the surface sink strengths for interstitials and vacancies can be considered nearly identical, $k_{sv}^2 = k_{si}^2$.

In situ irradiation experiment in this study was performed at room temperature, in the Stage III region (medium temperature regime) where individual self-interstitial atoms, vacancies and small interstitial clusters are mobile [6]. However, because of the existence of abundant free surfaces in NWs, it is reasonable to assume that the defect-surface interaction terms in the equations (1) and (2) are more dominant than the point defect recombination terms [37]. Therefore, at steady state where $\partial C_v/\partial t = \partial C_i/\partial t = 0$, the vacancy and interstitial concentrations C_v and C_i can be approximated by the following equations:

$$C_v = K_0/k_{sv}^2 D_v \quad (3)$$

$$C_i = K_0/k_{si}^2 D_i. \quad (4)$$

k_{sv}^{-1} and k_{si}^{-1} are defined as the mean distances of a vacancy and an interstitial traveling in the NWs before being trapped by the free surface [5, 36]. Both k_{sv}^2 and k_{si}^2 are proportional to $1/D^2$ where D is the diameter of Ag NWs. Therefore, during the steady state irradiation, the point defect concentration in 81 nm NW is nearly four times larger than that in 37 nm NW. It is known that the formation of defect clusters is determined by the supersaturation of point defects and the growth of defect clusters is controlled by the net accumulation rate of point defects to clusters [5]. Accordingly, a higher point defect concentration will trigger the formation of more and larger defect clusters in larger NWs, in good agreement with the experimental observations. In other words, if D is extremely small, the point defect density may be very low during irradiation (due to surface sinks) so that the accumulation of point defects and the subsequent formation of stable defect clusters in NWs may become very difficult. *In situ* Kr ion irradiation study by Sun *et al* revealed nearly defect-free ZnO NWs with diameter of 30 nm or less [15].

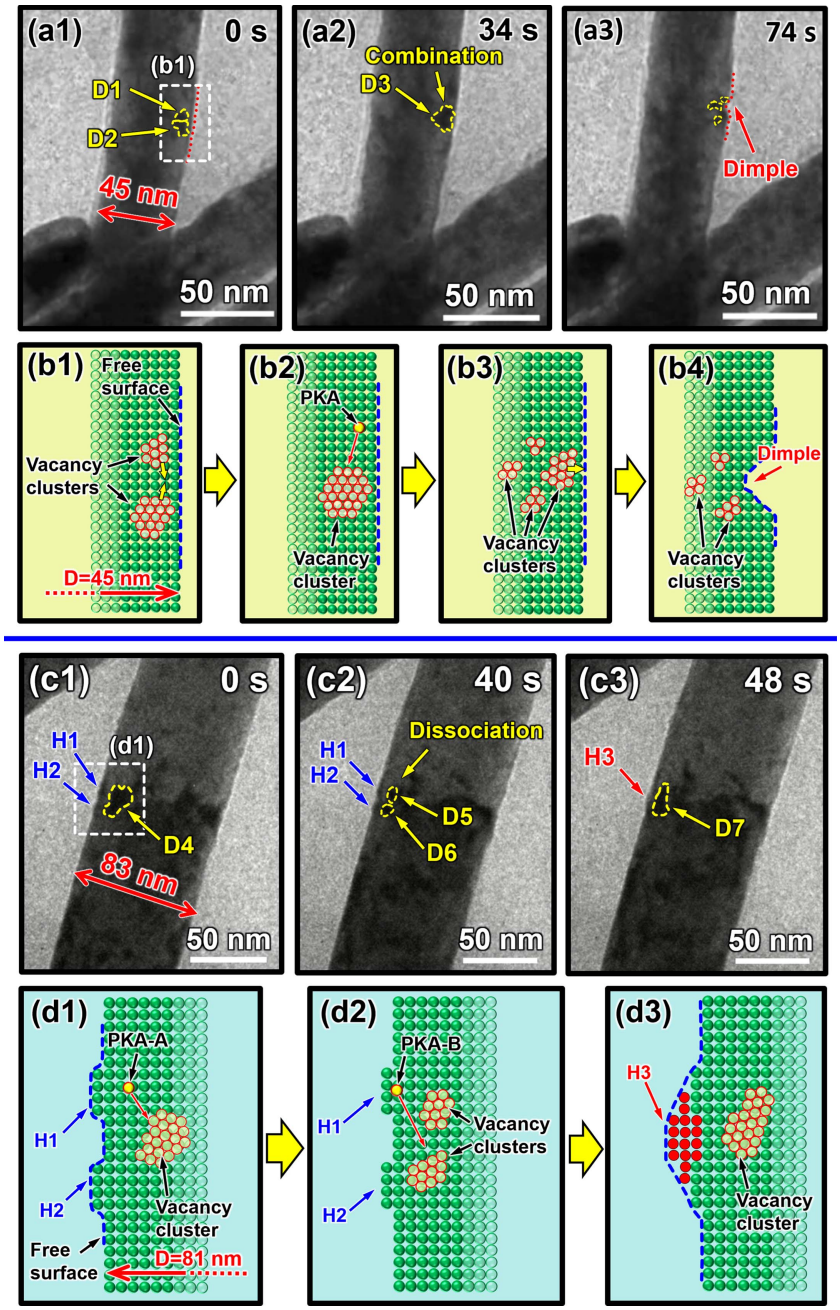

Figure 4. (a1)–(a3) *In situ* video snap shots showing the interactions between defect clusters and free surface in a Ag NW with a diameter of 45 nm over 0.91–0.94 dpa forming a surface dimple. Two defect clusters D1 and D2 combined with each other forming a larger cluster D3 from 0 to 34 s. After 40 s, D3 was partially absorbed by the surface, forming a dimple. Meanwhile the remaining of D3 dissociated into several smaller defect clusters. (b1)–(b4) The schematic diagram indicates the evolution of vacancy clusters within the area labeled by the white rectangular square in figure 4(a1), and the formation of a surface dimple due to the absorption of a large vacancy cluster. (c1)–(c3) *In situ* video snap shots indicating the interaction between defect clusters with free surface in a Ag NW with a diameter of 83 nm over 0.67–0.69 dpa and the consequent formation of a hump. At 0 s, a defect cluster D4 formed near two preexisting humps H1 and H2. By 40 s, D4 decomposed into two smaller clusters D5 and D6. By 48 s, D5 and D6 combined into a larger defect cluster D7, meanwhile a new hump H3 formed between H1 and H2 on the left surface of the NW. (d1)–(d3) The schematic diagram shows the evolution of vacancy clusters within the area labeled by the white rectangular square in figure 4(c1) and the interaction of an interstitial cluster with free surface, forming a new hump between two preexisting humps on wire surface.

4.2. Defect cluster types near the free surface

Recent MD simulation studies have shown that displacement cascades formed during irradiation can be described by local melted zones with a dimension of <5 nm in a short duration of time (<10 ps) [38, 39]. Within the cascade, interstitials tend to cluster on the periphery of the cascade [40, 41]. However, highly constrained vacancies tend to cluster within the core of the locally melted cascade [42, 43]. Different from electron and light ion irradiations, damages produced by heavy ion irradiation are mainly dense cascades and the distributions of interstitials and vacancies are highly segregated

rather than isolated Frenkel pairs, and subsequent quenching leads to formation of abundant defect clusters [5, 44].

Both *in situ* irradiation experiments and MD simulations on heavy ion irradiated Cu have shown that most (~90%) of the defect clusters observed in the region close to free surface are vacancy clusters [45, 46]. Studies have shown that the vacancy migration energy (E_m^v) in Ag is in the range of 0.83–1.03 eV, which is much larger than the interstitial migration energy (E_m^i), 0.03–0.1 eV [47–50]. Calculations also show that the migration activation energy of small vacancy clusters is ~0.19 eV in Ag, comparing to 0.05 eV for small interstitial clusters [51]. It is likely that a majority of defect clusters formed near the free surface ((D1)–(D7)) in irradiated Ag NWs illustrated in figure 4 are also vacancy clusters, as interstitials and small interstitial clusters may be absorbed by free surface, leaving behind relatively immobile vacancies and vacancy clusters in the cascade core.

An MD simulation study on Au NWs showed that the number of vacancies increased dramatically from NW surface, and reached a maximum at 4.5 nm. In comparison there is an interstitial free region, ~3.5 nm from the surface, beyond which the number of interstitials increased slightly [32]. In the present *in situ* irradiation study on Ag NWs, since the defect clusters labeled in figure 4 are located within the region several nm away from surface, they are more likely to be vacancy clusters. However, in the center of Ag NWs, there is a higher possibility to observe interstitial clusters.

4.3. Size-dependent surface roughening

In situ video snap shots in figure 4 indicate that the irradiation induced roughening of free surfaces may be attributed to the frequent interaction of defect clusters with free surfaces. However, it is noted that all defect clusters ((D1)–(D7)) in figure 4 were relatively immobile, a common characteristic of vacancy clusters, and they lingered near free surface for a relatively long period of time (40 s) without being captured by the free surface. It is possible that interactions between defect clusters with surface are facilitated by displacement cascade induced by incident Kr ions or PKAs. Extensive studies have shown that, during heavy ion irradiation, displacement cascades near surface can trigger viscous flow or microexplosions and thus modify the surface morphology by forming craters and extra atoms on the surface [52–56]. In the present *in situ* irradiation study, the total fluence is 2×10^{14} ions cm^{-2} and the flux was calculated to be 1×10^{11} ions cm^2 s^{-1}, indicating that there are ~10 Kr ions bombarding the Ag NWs per 100 nm^2 s^{-1}. The incident Kr ions or PKAs may either break the preexisting vacancy cluster into several smaller clusters or produce a displacement cascade near the vacancy cluster, facilitating the interaction of vacancy clusters with free surface via viscous flow or microexplosions.

Figures 4(b1)–(b4) are the schematic diagrams illustrating the formation of a small dimple on the surface of the 45 nm NW. As shown in figure 4(b1), two small vacancy clusters combine with each other forming a larger cluster. After lingering near the free surface for some time, the large vacancy cluster is dismantled by an energetic Kr ion, and breaks into four smaller vacancy clusters, one of which is immediately absorbed by the free surface forming a dimple, leaving behind three smaller ones. Figures 4(d1)–(d3) illustrate the formation of a small hump on the surface of the 81 nm NW. As shown in figure 4(d1), a large vacancy cluster emerges near the free surface. The defect cluster split into two vacancy clusters presumably due to a PKA or incident Kr ion. Soon after the dissociation, another PKA produces a displacement cascade near the two vacancy clusters. The highly mobile interstitials and interstitial clusters on the periphery of cascade migrate to surface and fill in the gap between two preexisting humps. The remaining vacancy cluster combines with the other two clusters to form a larger vacancy clusters. In the present study, both vacancy and interstitial clusters produced during the displacement cascade can interact with free surface leading to the morphology variation of the surface. However, most interstitials interact with surface in form of individual interstitial atom or small interstitials clusters. Due to their high mobility and relatively small size in Ag NWs, the absorption of interstitial clusters by free surface is difficult to resolve by *in situ* TEM observation. The continuous capture of smaller interstitial clusters and relatively large vacancy clusters by the free surface causes the accumulation of humps and dimples on the NW surface. Although surface roughening may also take place by forming zigzag surface facets without irradiation, the zigzag facets induced roughening were often formed during the synthesis process of twinned semiconducting NWs, such as Si, Ge, InP, GaAs, and the formation of highly periodic zigzag facets usually requires the existence of vertical or inclined TB to the NW axis [57–61].

As indicated in figure 3(c), a size effect of irradiation induced surface roughness is discovered in Ag NWs, that is thicker NWs tend to experience more surface roughening than thinner NWs. This size-dependent phenomenon can be interpreted by considering the saturated defect cluster density and average defect cluster size in NWs with different diameters. The total number density of defect clusters in NWs with a larger ($\rho_{\text{total}}^{\text{L}}$) and a smaller ($\rho_{\text{total}}^{\text{S}}$) diameter can be described by the following equations:

$$\rho_{\text{total}}^{\text{L}} = \rho_{\text{gen}} - \rho_{\text{com}}^{\text{L}} - \rho_{\text{sink}}^{\text{L}} \quad (5)$$

$$\rho_{\text{total}}^{\text{S}} = \rho_{\text{gen}} - \rho_{\text{com}}^{\text{S}} - \rho_{\text{sink}}^{\text{S}}, \quad (6)$$

where ρ_{gen} is the number density of defect clusters generated during irradiation. $\rho_{\text{com}}^{\text{L}}$ and $\rho_{\text{com}}^{\text{S}}$ are the number densities of defect clusters annihilated by mutual recombination of vacancy and interstitial clusters in larger and smaller NWs, respectively. $\rho_{\text{sink}}^{\text{L}}$ and $\rho_{\text{sink}}^{\text{S}}$ are the respective number density of defect clusters captured by free surface in larger and smaller wires.

As the irradiation temperature in the present study can cause mostly the migration of small interstitial clusters, the possibility of cluster recombination is small, and we ignore $\rho_{\text{com}}^{\text{L}}$ and $\rho_{\text{com}}^{\text{S}}$. Since the irradiation conditions are the same for NWs with different diameters, production term ρ_{gen} in all

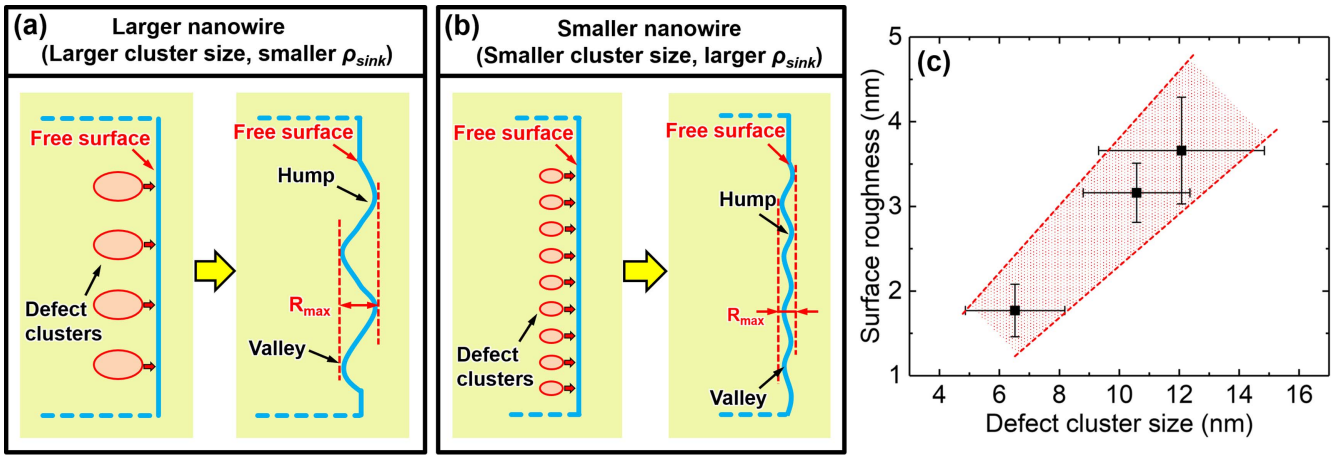

Figure 5. Schematic diagrams of the interaction of defect clusters with free surfaces in (a) larger NW and (b) smaller NW. Defect clusters are larger in Ag NW with larger diameter, and hence the absorption of defect cluster by free surface leads to greater surface roughness. Similarly the surface roughness is much less in smaller wires due to the smaller defect size. (c) Statistic data shows an increasing tendency of surface roughness in NWs with the average defect cluster size.

NWs is assumed to be similar. The measured defect density ρ_{total} is greater in larger wires $\rho^{L}_{total} > \rho^{S}_{total}$, indicating that the density of defect clusters absorbed by free surface is less in larger wire, i.e. $\rho^{L}_{sink} < \rho^{S}_{sink}$. The schematic diagrams in figures 5(a) and (b) show the influences of defect cluster density and average defect cluster size on the surface roughness in Ag NWs. Thicker NWs (such as those with 80 nm in diameter) contain larger defect clusters, and the absorption of these defect clusters by free surface will induce greater surface roughness. In addition, the relatively low cluster density leads to more irregularity on wire surfaces, as shown in figure 5(a). In comparison, smaller defect clusters are captured by free surfaces in thinner wires. The frequent interactions of vacancy clusters and interstitials clusters with free surface lead to moderate surface roughening (figure 5(b)), and thus enhance the radiation tolerance of NWs more effectively. As shown in figure 5(c), the surface roughness in NWs scales approximately with the average defect clusters size, providing indirect evidence for foregoing hypothesis.

5. Conclusion

In situ Kr ion irradiation experiments were performed to study the microstructural evolution and surface morphology variation with radiation dose in Ag NWs at room temperature. The major findings are summarized as follows: (1) Ag NWs exhibit a lower saturated defect cluster density during irradiation than CG Ag because of high fraction of free surfaces. (2) The NW surfaces gradually become rougher during irradiation up to 1 dpa due to the frequent interaction of defect clusters with free surface. (3) A size-dependent surface roughening phenomenon was observed in Ag NWs with difference diameters. The possible underlying mechanism is attributed to the size dependent defect cluster density and average defect cluster size and the existence of SAZs.

Acknowledgments

We acknowledge financial support by NSF-CMMI Program under grant no. 1728419. CF is supported by NSF-DMR 1643915. TDS is supported by the National Natural Science Foundation of China (Grant No. 11575154) and the High-level Talents Research Program of the Yanshan University (Grant No. 606001101). We also thank Peter M Baldo and Edward A Ryan at Argonne National Laboratory for their help during *in situ* irradiation experiments. The IVEM facility at Argonne National Laboratory is supported by DOE-Office of Nuclear Energy. Access to the Microscopy Center at Purdue University is acknowledged. This work was also performed, in part, at the Center for Integrated Nanotechnologies (CINT), an Office of Science User Facility operated for the US Department of Energy (DOE), Office of Science by Los Alamos National Laboratory (Contract DE-AC52-06NA25396) and Sandia National Laboratories (Contract DE-NA-0003525).

ORCID iDs

Z Shang https://orcid.org/0000-0002-2974-2599

References

[1] Zinkle S J and Was G 2013 Materials challenges in nuclear energy *Acta Mater.* **61** 735–58
[2] Chu S and Majumdar A 2012 Opportunities and challenges for a sustainable energy future *Nature* **488** 294
[3] Abram T and Ion S 2008 Generation-IV nuclear power: a review of the state of the science *Energy Policy* **36** 4323–30
[4] Murty K and Charit I 2008 Structural materials for Gen-IV nuclear reactors: challenges and opportunities *J. Nucl. Mater.* **383** 189–95
[5] Was G S 2016 *Fundamentals of Radiation Materials Science: Metals and Alloys* (Berlin: Springer)

[6] Zinkle S J 2012 1.03-radiation-induced effects on microstructure *Comprehensive Nuclear Materials* vol 1 (Oxford: Elsevier) pp 65–98

[7] Hoffelner W 2012 *Materials for Nuclear Plants: From Safe Design to Residual Life Assessments* (Berlin: Springer)

[8] Ackland G 2010 Controlling radiation damage *Science* **327** 1587–8

[9] Bai X-M, Voter A F, Hoagland R G, Nastasi M and Uberuaga B P 2010 Efficient annealing of radiation damage near grain boundaries via interstitial emission *Science* **327** 1631–4

[10] Han W, Demkowicz M, Fu E, Wang Y and Misra A 2012 Effect of grain boundary character on sink efficiency *Acta Mater.* **60** 6341–51

[11] Beyerlein I, Caro A, Demkowicz M, Mara N, Misra A and Uberuaga B 2013 Radiation damage tolerant nanomaterials *Mater. Today* **16** 443–9

[12] Sun C, Zheng S, Wei C, Wu Y, Shao L, Yang Y, Hartwig K, Maloy S, Zinkle S and Allen T 2015 Superior radiation-resistant nanoengineered austenitic 304L stainless steel for applications in extreme radiation environments *Sci. Rep.* **5** 7801

[13] Yu K, Bufford D, Sun C, Liu Y, Wang H, Kirk M, Li M and Zhang X 2013 Removal of stacking-fault tetrahedra by twin boundaries in nanotwinned metals *Nat. Commun.* **4** 1377

[14] Sun C, Bufford D, Chen Y, Kirk M A, Wang Y Q, Li M, Wang H, Maloy S A and Zhang X 2014 *In situ* study of defect migration kinetics in nanoporous Ag with enhanced radiation tolerance *Sci. Rep.* **4** 3737

[15] Sun C, Uberuaga B, Yin L, Li J, Chen Y, Kirk M, Li M, Maloy S, Wang H and Yu C 2015 Resilient ZnO nanowires in an irradiation environment: an *in situ* study *Acta Mater.* **95** 156–63

[16] Li J, Fan C, Ding J, Xue S, Chen Y, Li Q, Wang H and Zhang X 2017 *In situ* heavy ion irradiation studies of nanopore shrinkage and enhanced radiation tolerance of nanoporous Au *Sci. Rep.* **7** 39484

[17] Bringa E M, Monk J, Caro A, Misra A, Zepeda-Ruiz L, Duchaineau M, Abraham F, Nastasi M, Picraux S and Wang Y 2011 Are nanoporous materials radiation resistant? *Nano Lett.* **12** 3351–5

[18] Li J, Chen Y, Wang H and Zhang X 2018 *In situ* study on enhanced heavy ion irradiation tolerance of porous Mg *Scr. Mater.* **144** 13–7

[19] Li J, Fan C, Li Q, Wang H and Zhang X 2018 *In situ* studies on irradiation resistance of nanoporous Au through temperature-jump tests *Acta Mater.* **143** 30–42

[20] Zhu Y, Qin Q, Xu F, Fan F, Ding Y, Zhang T, Wiley B J and Wang Z L 2012 Size effects on elasticity, yielding, and fracture of silver nanowires: *in situ* experiments *Phys. Rev.* B **85** 045443

[21] Filleter T, Ryu S, Kang K, Yin J, Bernal R A, Sohn K, Li S, Huang J, Cai W and Espinosa H D 2012 Nucleation-controlled distributed plasticity in penta-twinned silver nanowires *Small* **8** 2986–93

[22] Liu W, Chen P, Qiu R, Khan M, Liu J, Hou M and Duan J 2017 A molecular dynamics simulation study of irradiation induced defects in gold nanowire *Nucl. Instrum. Methods Phys. Res.* B **405** 22–30

[23] Lee J-Y, Connor S T, Cui Y and Peumans P 2008 Solution-processed metal nanowire mesh transparent electrodes *Nano Lett.* **8** 689–92

[24] Wu H, Kong D, Ruan Z, Hsu P-C, Wang S, Yu Z, Carney T J, Hu L, Fan S and Cui Y 2013 A transparent electrode based on a metal nanotrough network *Nat. Nanotechnol.* **8** 421–5

[25] Garnett E C, Cai W, Cha J J, Mahmood F, Connor S T, Christoforo M G, Cui Y, McGehee M D and Brongersma M L 2012 Self-limited plasmonic welding of silver nanowire junctions *Nat. Mater.* **11** 241–9

[26] Sun M, Cao R, Xiao F and Deng C 2013 Surface and interface controlled yielding and plasticity in fivefold twinned Ag nanowires *Comput. Mater. Sci.* **79** 289–95

[27] Sun M, Cao R, Xiao F and Deng C 2013 Five-fold twin and surface groove-induced abnormal size-and temperature-dependent yielding in Ag nanowires *Scr. Mater.* **69** 227–30

[28] Birtcher R, Kirk M, Furuya K, Lumpkin G and Ruault M 2005 *In situ* transmission electron microscopy investigation of radiation effects *J. Mater. Res.* **20** 1654–83

[29] Ziegler J F, Biersack J P and Littmark U 1995 *The Stopping and Range of Ions in Matter* (New York: Pergamon)

[30] Stoller R E, Toloczko M B, Was G S, Certain A G, Dwaraknath S and Garner F A 2013 On the use of SRIM for computing radiation damage exposure *Nucl. Instrum. Methods Phys. Res.* B **310** 75–80

[31] Ziegler J F, Ziegler M D and Biersack J P 2010 SRIM–The stopping and range of ions in matter (2010) *Nucl. Instrum. Methods Phys. Res.* B **268** 1818–23

[32] Zhang C, Li Y, Zhou W, Hu L and Zeng Z 2015 Anti-radiation mechanisms in nanoporous gold studied via molecular dynamics simulations *J. Nucl. Mater.* **466** 328–33

[33] Barnett D and Lothe J 1974 An image force theorem for dislocations in anisotropic bicrystals *J. Phys. F: Met. Phys.* **4** 1618

[34] Li J, Chen Y, Wang H and Zhang X 2017 *In situ* studies on twin-thickness-dependent distribution of defect clusters in heavy ion-irradiated nanotwinned Ag *Metall. Mater. Trans.* A **48** 1466–73

[35] Li J, Yu K, Chen Y, Song M, Wang H, Kirk M, Li M and Zhang X 2015 *In situ* study of defect migration kinetics and self-healing of twin boundaries in heavy ion irradiated nanotwinned metals *Nano Lett.* **15** 2922–7

[36] Brailsford A and Bullough R 1972 The rate theory of swelling due to void growth in irradiated metals *J. Nucl. Mater.* **44** 121–35

[37] Shen T 2008 Radiation tolerance in a nanostructure: is smaller better ? *Nucl. Instrum. Methods Phys. Res.* B **266** 921–5

[38] De La Rubia T D, Averback R S, Benedek R and King W 1987 Role of thermal spikes in energetic displacement cascades *Phys. Rev. Lett.* **59** 1930

[39] Bacon D J and de la Rubia T D 1994 Molecular dynamics computer simulations of displacement cascades in metals *J. Nucl. Mater.* **216** 275–90

[40] Foreman A, Phythian W and English C 1992 The molecular dynamics simulation of irradiation damage cascades in copper using a many-body potential *Philos. Mag.* A **66** 671–95

[41] de la Rubia T D and Phythian W 1992 Molecular dynamics studies of defect production and clustering in energetic displacement cascades in copper *J. Nucl. Mater.* **191** 108–15

[42] de la Rubia T D 1996 Irradiation-induced defect production in elemental metals and semiconductors: a review of recent molecular dynamics studies *Annu. Rev. Mater. Sci.* **26** 613–49

[43] Averback R S and de La Rubia T D 1997 Displacement damage in irradiated metals and semiconductors *Solid State Phys.* **51** 281–402

[44] Woo C and Singh B 1992 Production bias due to clustering of point defects in irradiation-induced cascades *Philos. Mag.* A **65** 889–912

[45] Nordlund K, Keinonen J, Ghaly M and Averback R S 1999 Coherent displacement of atoms during ion irradiation *Nature* **398** 49–51

[46] Fukushima H, Jenkins M and Kirk M 1997 On the determination of the nature of defect clusters produced by displacement cascades: II. Application of stereo imaging techniques to heavy-ion damage in copper *Philos. Mag.* A **75** 1583–602

[47] Wynblatt P 1968 Calculation of the vacancy migration energy in cubic crystals *J. Phys. Chem. Solids* **29** 215–24

[48] Lam N, Dagens L and Doan N 1983 Calculations of the properties of self-interstitials and vacancies in the face-centred cubic metals Cu, Ag and Au *J. Phys. F: Met. Phys.* **13** 2503
[49] Seeger A, Schottky G and Schumacher D 1965 The contribution of multiple vacancies to self-diffusion *Phys. Stat. Sol.* **11** 363–70
[50] Schilling W 1978 Self-interstitial atoms in metals *J. Nucl. Mater.* **69** 465–89
[51] Lam N, Doan N and Dagens L 1985 Multiple defects in copper and silver *J. Phys. F: Met. Phys.* **15** 799
[52] Ghaly M, Nordlund K and Averback R 1999 Molecular dynamics investigations of surface damage produced by kiloelectronvolt self-bombardment of solids *Philos. Mag.* A **79** 795–820
[53] Birtcher R and Donnelly S 1996 Plastic flow induced by single ion impacts on gold *Mater. Res. Soc. Proc.* **439** 4374
[54] Donnelly S and Birtcher R 1997 Heavy ion cratering of gold *Phys. Rev.* B **56** 13599
[55] Ghaly M and Averback R 1994 Effect of viscous flow on ion damage near solid surfaces *Phys. Rev. Lett.* **72** 364
[56] Greaves G, Hinks J, Busby P, Mellors N, Ilinov A, Kuronen A, Nordlund K and Donnelly S 2013 Enhanced sputtering yields from single-ion impacts on gold nanorods *Phys. Rev. Lett.* **111** 065504
[57] Banerjee R, Bhattacharya A, Genc A and Arora B 2006 Structure of twins in GaAs nanowires grown by the vapour–liquid–solid process *Philos. Mag. Lett.* **86** 807–16
[58] Algra R E, Verheijen M A, Borgström M T, Feiner L-F, Immink G, van Enckevort W J, Vlieg E and Bakkers E P 2008 Twinning superlattices in indium phosphide nanowires *Nature* **456** 369
[59] Arbiol J, Fontcuberta i Morral A, Estradé S, Peiró F, Kalache B, Roca i Cabarrocas P and Morante J R 2008 Influence of the (111) twinning on the formation of diamond cubic/diamond hexagonal heterostructures in Cu-catalyzed Si nanowires *J. Appl. Phys.* **104** 064312
[60] Caroff P, Dick K A, Johansson J, Messing M E, Deppert K and Samuelson L 2009 Controlled polytypic and twin-plane superlattices in III–V nanowires *Nat. Nanotechnol.* **4** 50
[61] Ross F, Tersoff J and Reuter M 2005 Sawtooth faceting in silicon nanowires *Phys. Rev. Lett.* **95** 146104